

# Questioning the wobbling interpretation of low-spin bands in $\gamma$ -soft nuclei within the interacting boson-fermion model

K. Nomura<sup>1,\*</sup> and C. M. Petrache<sup>2</sup>

<sup>1</sup>*Department of Physics, Faculty of Science, University of Zagreb, HR-10000, Croatia*

<sup>2</sup>*Université Paris-Saclay, CNRS/IN2P3, IJCLab, 91405 Orsay, France*

(Dated: February 15, 2022)

An alternative interpretation of the recently reported low-lying excited bands in  $\gamma$ -soft odd-mass nuclei as wobbling bands is presented in terms of the interacting boson-fermion model. The model Hamiltonian is determined based on the mean-field calculations with the nuclear energy density functionals. The predicted mixing ratios of the  $\Delta I = 1$  electric quadrupole to magnetic dipole transition rates between yrast bands and those yrare bands previously interpreted as wobbling bands in  $^{135}\text{Pr}$ ,  $^{133}\text{La}$ ,  $^{127}\text{Xe}$ , and  $^{105}\text{Pd}$  are consistently smaller in magnitude than the experimental values on which the wobbling interpretation is based. These calculated mixing ratios indicate predominant magnetic character in agreement with the new experimental data. The earlier wobbling assignments are severely questioned.

## I. INTRODUCTION

Ground-state shape of most nonspherical nuclear systems is characterized by axially-symmetric quadrupole deformation [1]. The axial symmetry, i.e., invariance under rotation about the symmetry axis of the intrinsic frame, is, however, broken in many nuclei. The nonaxial nuclear shapes as well as the resulting triaxially deformed rotors are a prominent feature of nuclear structure. A fingerprint of the rigid triaxiality is wobbling motion [1], a collective mode in which the principal axis of a triaxial rotor corresponding to the largest moment of inertia oscillates about the space-fixed angular momentum. The phenomenon has attracted much attention in nuclear physics, and is also recognized in finite many-body microscopic and macroscopic systems in general.

The wobbling motion in nuclei can be identified experimentally through the observation of rotational bands that are connected to each other by predominant  $\Delta I = 1$  electric quadrupole ( $E2$ ) transitions, because the collective oscillation of the entire nuclear charge is involved. Traditionally, excited bands that manifest features of wobbling motion have been identified in high-spin bands of the odd-mass Lu and Ta nuclei in the mass  $A \approx 160$  region [2–7]. More recent experiments have shown new evidence for wobbling bands in odd-mass nuclei in several other mass regions, observed in the low-spin regime, e.g., in  $^{135}\text{Pr}$  [8, 9],  $^{133}\text{La}$  [10],  $^{105}\text{Pd}$  [11],  $^{127}\text{Xe}$  [12],  $^{187}\text{Au}$  [13], and  $^{183}\text{Au}$  [14], as well as at medium spins in  $^{130}\text{Ba}$  [15] and  $^{136}\text{Nd}$  [16]. In comparison to the high-spin wobbling bands of strongly-deformed triaxial nuclei in the mass  $A \approx 160$  region, the new experiments have proposed the occurrence of low-spin wobbling motion in normal-deformed  $\gamma$ -soft nuclei, which are characterized by a collective potential that is soft in nonaxial deformation and has small quadrupole deformation. The search for new regions of wobbling motion expands the frontier

of nuclear collective motion, but should be accompanied by increasing experimental rigour.

In fact, it is of crucial importance to critically assess the reported experimental evidence for the wobbling bands. The wobbling interpretation requires connecting transitions with predominant electric character, which can be established by extracting mixing ratios  $\delta(E2/M1)$  with magnitudes larger than 1, which signifies predominance of the electric over the magnetic components. Actually, new experiments that involve angular distribution combined with linear polarization measurements on excited bands in  $^{187}\text{Au}$  [17] and  $^{135}\text{Pr}$  [18] showed that the interband transition between the proposed wobbling bands and the yrast bands in these nuclei are predominantly magnetic. The wobbling interpretation of the newly found bands has been mostly based on a particle-rotor picture, in which the configuration that embodies the wobbling motion is explicitly considered within the intrinsic frame of reference [8–11, 18, 19]. On the other hand, it would be useful to give an alternative theoretical interpretation of the proposed low-spin wobbling bands if the character of the connecting transitions is not predominantly electric, as required by the collective wobbling motion.

In this paper, we shall consider the recently proposed low-spin wobbling bands of  $\gamma$ -soft odd-mass nuclei  $^{135}\text{Pr}$ ,  $^{133}\text{La}$ ,  $^{127}\text{Xe}$ , and  $^{105}\text{Pd}$ , within the interacting boson-fermion model (IBFM) [20, 21], with the Hamiltonian determined by the constrained mean-field calculations that are based upon the nuclear energy density functional (EDF) [22–25]. The aim of this work is to provide an alternative interpretation of the observed non-yrast bands of the above odd-mass nuclei. Our calculation reproduces the new data on  $^{135}\text{Pr}$  [18] and the old data on  $^{105}\text{Pd}$  [26], but is in contradiction with those experimental data on which the wobbling interpretation is based. Here we mainly focus on the excitation spectra and electromagnetic transition properties of these non-yrast bands, that are obtained from the diagonalization of the IBFM Hamiltonian in the laboratory frame of ref-

\* knomura@phy.hr

erence. We also note that certain intrinsic properties of odd-mass nuclei can be dealt with within the IBFM framework as well, by making use of the formalism of coherent state that is generalized to coupled boson-fermion systems [21, 27, 28]. This procedure has been extensively used for analyzing properties in the intrinsic frame, including the studies of the quantum shape-phase transitions in odd-mass nuclei [29, 30].

The paper is organized as follows. In Sec. II, we outline the theoretical procedure to construct the IBFM Hamiltonian based on the mean-field calculations. Section III shows our results including the excitation spectra,  $E2/M1$  mixing ratios,  $B(E2)$  and  $B(M1)$  transitions for the considered odd-mass nuclei  $^{135}\text{Pr}$ ,  $^{133}\text{La}$ ,  $^{127}\text{Xe}$ , and  $^{105}\text{Pd}$ . Summary of the main results is given in Sec. IV.

## II. THEORETICAL PROCEDURE

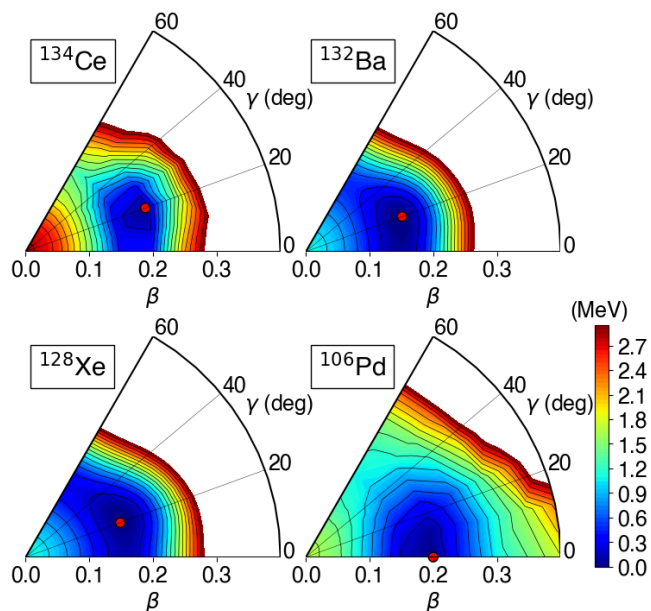


FIG. 1. Potential energy surfaces (PESs) for the even-even core nuclei obtained from the mean-field calculations with quadrupole degrees of freedom  $\beta$  and  $\gamma$ . Two representative nuclear effective interactions are employed: Gogny D1M [31] (for  $^{132}\text{Ba}$ , and  $^{128}\text{Xe}$ ) and DD-PC1 [32] (for  $^{134}\text{Ce}$  and  $^{106}\text{Pd}$ ) EDFs. The total mean-field energies are plotted up to 3 MeV, normalized with respect to the global minimum which is represented by a solid circle. The energy difference between the neighboring contours is 0.2 MeV. Note the PESs for  $^{132}\text{Ba}$  and  $^{128}\text{Xe}$  are taken from Ref. [33].

In even-even nuclei, to a good approximation, nucleons are coupled pairwise and the presence of such pairs play an important role in nuclear dynamics, determining basic parameters of vibrational and rotational spectra. In odd-mass nuclear systems, one has to consider explicitly

the unpaired nucleon and treat the collective and noncollective (single-particle) degrees of freedom on the same footing [34]. A major assumption in the present work is that the low-lying states of an even-even nucleus is described by the interacting boson model (IBM) [35], consisting of the monopole  $s$  (with spin and parity  $L = 0^+$ ) and quadrupole  $d$  ( $L = 2^+$ ) bosons, which represent the collective  $S$  and  $D$  pairs of valence nucleons, respectively.

The low-energy structure of a given odd-mass nucleus is determined by the interaction between an odd fermion and the even-even boson (IBM) core. Specifically,  $^{135}\text{Pr}$  ( $^{133}\text{La}$ ) is a system composed of even-even core  $^{134}\text{Ce}$  ( $^{132}\text{Ba}$ ) plus an odd proton particle, while  $^{127}\text{Xe}$  ( $^{105}\text{Pd}$ ) is composed of the  $^{128}\text{Xe}$  ( $^{106}\text{Pd}$ ) even-even core coupled to the odd neutron hole. For all these odd-mass nuclei, the fermion space corresponds to the proton  $Z$  or neutron  $N = 50 - 82$  major oscillator shell, hence only the orbital  $1h_{11/2}$  is considered to describe negative-parity states. In general, the IBFM Hamiltonian is given by

$$\hat{H} = \hat{H}_B + \hat{H}_F + \hat{V}_{BF}, \quad (1)$$

where  $\hat{H}_B$  stands for the IBM Hamiltonian for an even-even core,  $\hat{H}_F$  is the single-nucleon Hamiltonian, and  $\hat{V}_{BF}$  represents the boson-fermion interaction.

In the first step of the present theoretical analysis, we carry out, for each even-even core nucleus, the constrained mean-field calculations [36] based on a given EDF, and obtain the potential energy surface (PES) with triaxial quadrupole degrees of freedom. The constraints imposed here are on the mass quadrupole moments that are associated with the polar deformation parameters  $\beta$  and  $\gamma$  ( $0^\circ \leq \gamma \leq 60^\circ$ ) [37]. Two types of the mean-field methods are considered: (i) the Hartree-Fock-Bogoliubov method [24] with the parametrization D1M [31] of the Gogny EDF [38] for  $^{132}\text{Ba}$  and  $^{128}\text{Xe}$ ; (ii) the relativistic Hartree-Bogoliubov method [23] with the density-dependent point-coupling (DD-PC1) EDF [32] for particle-hole channel and the separable pairing force of finite range [39] for the particle-particle channel for  $^{134}\text{Ce}$  and  $^{106}\text{Pd}$ . The calculated PESs for the even-even nuclei  $^{134}\text{Ce}$ ,  $^{132}\text{Ba}$ ,  $^{128}\text{Xe}$ , and  $^{106}\text{Pd}$ , shown in Fig. 1, are essentially soft in  $\gamma$  deformation. This situation is characteristic of the  $\gamma$ -unstable rotor picture [40], which is also equivalent to the  $O(6)$  limit of the IBM.

In the next step we build the IBM Hamiltonian  $\hat{H}_B$ . In this study, we employ the proton-neutron IBM (IBM-2) [41]. The IBM-2 comprises the proton  $s_\pi$  and  $d_\pi$  bosons, and the neutron  $s_\nu$  and  $d_\nu$  bosons, which represent the collective monopole and quadrupole proton-proton and neutron-neutron pairs, respectively. For the IBM Hamiltonian  $\hat{H}_B$  we adopt the form

$$\hat{H}_B = \epsilon_d(\hat{n}_{d_\pi} + \hat{n}_{d_\nu}) + \kappa \hat{Q}_\pi \cdot \hat{Q}_\nu, \quad (2)$$

where in the first term  $\hat{n}_{d_\rho} = \hat{d}_\rho^\dagger \cdot \hat{d}_\rho$  ( $\rho = \pi$  or  $\nu$ ), represents the number operator for the  $d_\rho$  bosons, with  $\epsilon_d$  the single  $d$ -boson energy relative to the  $s$ -boson one, and  $\hat{d}_\mu = (-1)^\mu \hat{d}_{-\mu}$ .  $\hat{Q}_\rho = s_\rho^\dagger \hat{d}_\rho + \hat{d}_\rho^\dagger \hat{s}_\rho + \chi_\rho(\hat{d}_\rho^\dagger \times \hat{d}_\rho)^{(2)}$  is the

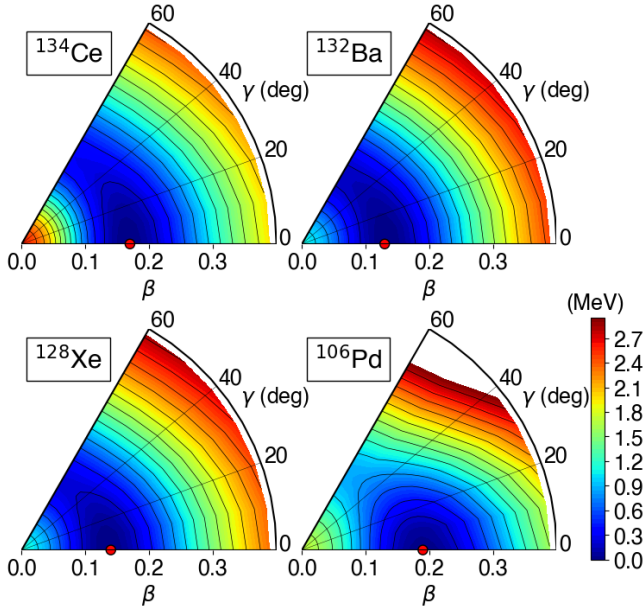


FIG. 2. Same as Fig. 1, but for the bosonic PESs.

bosonic quadrupole operator.  $\epsilon_d$ ,  $\kappa$ ,  $\chi_\pi$ , and  $\chi_\nu$  are the parameters to be determined.

The geometrical structure of a given IBM Hamiltonian is studied by introducing the boson coherent state [42], which is given by

$$|\Phi\rangle = \prod_{\rho=\nu,\pi} \left[ s_\rho^\dagger + \sum_{\mu=-2}^{+2} \alpha_{\rho\mu} d_{\rho\mu}^\dagger \right]^{N_\rho} |0\rangle, \quad (3)$$

up to a normalization factor. The amplitudes  $\alpha_{\rho\mu}$  are given as  $\alpha_{\rho 0} = \beta_\rho \cos \gamma_\rho$ ,  $\alpha_{\rho \pm 1} = 0$ , and  $\alpha_{\rho \pm 2} = \beta_\rho \sin \gamma_\rho / \sqrt{2}$ , where  $\beta_\rho$  and  $\gamma_\rho$  are boson analogs of the deformation variables.  $N_\rho$  is the number of neutron ( $\rho = \nu$ ) or proton ( $\rho = \pi$ ) bosons, and  $|0\rangle$  represents the boson vacuum, i.e., the inert core. We assume that both proton and neutron bosons have equal deformations,  $\beta_\pi = \beta_\nu$  and  $\gamma_\pi = \gamma_\nu$ . We could, in general, take the deformations for the proton and neutron bosons to be different from each other [43, 44], and would then have to treat the energy surface in four dimensions both in the mean-field and IBM-2 frameworks. In practical calculations, however, comparison between the fermionic and bosonic PESs in the four dimensional spaces would be too complicated. To simplify the discussion, we here assume equal proton and neutron deformations for both fermion and boson systems. We further assume that the fermionic and bosonic deformations can be related to each other in such a way that  $\beta_\pi = \beta_\nu \propto \beta$  and  $\gamma_\pi = \gamma_\nu \equiv \gamma$  [42, 45].

The parameters of the boson Hamiltonian are determined by mapping the fermionic PES onto the expectation value of  $\hat{H}_B$  in the above coherent state, as in Ref. [45]. In other words, the IBM parameters are calibrated so that the fermionic and bosonic PESs become similar to

each other. No phenomenological adjustment to experiment is made in this procedure. We also note that the IBM Hamiltonian (2) is a rather specific form of the most general IBM-2 Hamiltonian. A more accurate theoretical description of the relevant spectroscopic properties of both even-even and odd-mass nuclei might require the inclusion of additional terms to  $\hat{H}_B$ , in particular, the so-called Majorana terms, which could play an important role in calculations of  $M1$  properties. The Majorana terms, however, do not add independent contributions to the energy surface, unless the proton and neutron deformations are taken to be different [44]. Under the present assumption that the deformations for the proton and neutron boson systems are equal to each other, the strength parameters of these terms cannot be determined only by the comparison of the fermionic and bosonic PESs that are given in terms of the  $\beta$  and  $\gamma$  degrees of freedom only.

In Fig. 2 we show the mapped (bosonic) PESs for the even-even core nuclei  $^{134}\text{Ce}$ ,  $^{132}\text{Ba}$ ,  $^{128}\text{Xe}$ , and  $^{106}\text{Pd}$ , which can be compared with the original fermionic PESs in Fig. 1. In general, the bosonic PES appears to be flat especially in the region far from the global minimum. This reflects the fact that the IBM is built on the valence space of collective nucleon pairs in one major shell, while the mean-field model involves all nucleons. The bosonic PESs for  $^{134}\text{Ce}$ ,  $^{132}\text{Ba}$ , and  $^{128}\text{Xe}$  exhibit a minimum on the prolate axis  $\gamma = 0^\circ$ , while a shallow triaxial minimum at  $\gamma \approx 20^\circ$  is suggested in the corresponding fermionic PESs. This discrepancy could be corrected by including a higher-order term in the IBM Hamiltonian [46]. However, the triaxial minimum in the fermionic PES is so shallow that the discrepancy is expected to have a minor influence on the low-lying spectra of odd-mass nuclei.

Having fixed the boson-core Hamiltonian, we introduce the unpaired nucleon degree of freedom. The single-nucleon Hamiltonian in Eq. (1) reads

$$\hat{H}_F = -\epsilon_{j_\rho} \sqrt{2j_\rho + 1} (a_{j_\rho}^\dagger \times \tilde{a}_{j_\rho})^{(0)} \equiv \epsilon_{j_\rho} \hat{n}_{j_\rho}, \quad (4)$$

where  $\epsilon_{j_\rho}$  is single-particle energy for the odd proton ( $\rho = \pi$ ) or neutron ( $\rho = \nu$ ) in orbital  $j_\rho$ ,  $a_{j_\rho}^{(\dagger)}$  denotes the operator that annihilate (create) a single nucleon with  $\tilde{a}_{j_\rho, m_\rho} = (-1)^{j_\rho - m_\rho} a_{j_\rho, -m_\rho}$ , and  $\hat{n}_{j_\rho}$  stands for the fermion number operator.

The interaction term  $\hat{V}_{BF}$  for the coupling between the odd nucleon with the angular momentum  $j_\rho$  and the boson core has the form

$$\begin{aligned} \hat{V}_{BF} = & \Gamma_{j_\rho} \hat{Q}_{\rho'} \cdot (a_{j_\rho}^\dagger \times \tilde{a}_{j_\rho})^{(2)} + \Lambda_{j_\rho} \left[ : (s_{\rho'}^\dagger \times \tilde{d}_{\rho'})^{(2)} \right. \\ & \cdot \left( (d_\rho^\dagger \times \tilde{a}_{j_\rho})^{(j_\rho)} \times (a_{j_\rho}^\dagger \times \tilde{s}_\rho)^{(j_\rho)} \right)^{(2)} : + (H.c.) \left. \right] \\ & + A_0 \hat{n}_{d_\rho} \hat{n}_{j_\rho}, \end{aligned} \quad (5)$$

where  $\rho' \neq \rho$ . The first, second, and third terms are the quadrupole dynamical, exchange, and monopole interactions, respectively. The  $j$ -dependent parameters  $\Gamma_{j_\rho}$  and

$\Lambda_{j\rho}$  are given by [21, 47]

$$\Gamma_{j\rho} = \Gamma_0(u_{j\rho}^2 - v_{j\rho}^2)Q_{j\rho j\rho} \quad (6a)$$

$$\Lambda_{j\rho} = \Lambda_0 \left[ -4u_{j\rho}^2 v_{j\rho}^2 Q_{j\rho j\rho}^2 \sqrt{\frac{10}{N_\rho(2j_\rho + 1)}} \right] \quad (6b)$$

$Q_{j\rho j\rho}$  stands for the matrix element of the spherical harmonic in the single-particle basis, i.e.,  $Q_{j\rho j\rho} = \langle l_{\rho \frac{1}{2} j_\rho} \| Y^{(2)} \| l_{\rho \frac{1}{2} j_\rho} \rangle$ , and  $u_{j\rho}^2 + v_{j\rho}^2 = 1$  is satisfied. The dots :  $(\dots)$  : in Eq. (5) denotes normal ordering. Based on the microscopic considerations in terms of the generalized seniority scheme [47], it is assumed that both the dynamical and exchange terms are dominated by the interaction between unlike particles, i.e., between the odd proton (neutron) and the neutron (proton) bosons. The exchange term takes into account the fact that the bosons are made of nucleon pairs. For the monopole term, the interaction between like-particles, i.e., between the odd proton (neutron) and the proton (neutron) bosons, is considered. The specific boson-fermion interaction of the form (5), which is based on the generalized seniority, has been frequently used in a number of phenomenological IBFM calculations including the spectroscopic studies of strongly deformed nuclei [21, 47, 48].

The building blocks of  $\hat{H}_F$  and  $\hat{V}_{BF}$  are spherical single-particle energy  $\epsilon_{j\rho}$  and occupation probability  $v_{j\rho}^2$  of the odd fermion with  $j = 11/2$ , which are computed by the same mean-field calculations constrained to zero deformation [49]. The three coupling constants  $\Gamma_0$ ,  $\Lambda_0$ , and  $A_0$ , defined in Eqs. (5) and (6), are fitted to reproduce to a reasonable accuracy the low-lying excitation energies of each odd-mass nucleus. Table I lists the adopted values of the parameters of  $\hat{H}_B$  (2), the occupation probability  $v^2$  of the odd particle, and the fitted coupling constants of  $\hat{V}_{BF}$ .

The IBFM Hamiltonian thus constructed is diagonalized in the basis  $[[L_\pi L_\nu(L); j : I]$  [50], where  $L_\pi$  ( $L_\nu$ ) and  $L$  are the angular momentum of proton (neutron) boson system, and the total angular momentum of the even-even boson core, respectively.  $I$  stands for the total angular momentum of the coupled boson-fermion system.

### III. RESULTS AND DISCUSSIONS

#### A. Excitation spectra

Now we turn to the discussion about the spectroscopic properties of low-spin bands in odd-mass nuclei, which are produced by the diagonalization of the IBFM Hamiltonian (1) with the parameters obtained by the aforementioned procedure. In what follows, the band built on the  $11/2_1^-$  state, the first, and the second excited bands resulting from the IBFM calculations are denoted by Yrast, B1, and B2, respectively.

In Fig. 3 the predicted five lowest-energy negative-parity bands of  $^{135}\text{Pr}$  are shown. The theoretical Yrast,

TABLE I. The parameters for the IBM Hamiltonian (2), the effective  $E2$  boson charge  $e^B$ , proton  $g_\pi^B$  and neutron  $g_\nu^B$  factors, and the occupation probability  $v_{j\rho}^2$  of the odd particle in the  $1h_{11/2}$  single-particle state, and the fitted coupling constants of  $\hat{V}_{BF}$ . The numbers of proton  $N_\pi$  and neutron  $N_\nu$  bosons are also shown, with bar representing hole nature.

	$^{135}\text{Pr}$	$^{133}\text{La}$	$^{127}\text{Xe}$	$^{105}\text{Pd}$
Boson core	$^{134}\text{Ce}$	$^{132}\text{Ba}$	$^{128}\text{Xe}$	$^{106}\text{Pd}$
$(N_\pi, N_\nu)$	(4, 3)	(3, 3)	(2, 4)	(2, 5)
$\epsilon_d$ (MeV)	0.3	0.650	0.62	0.70
$\kappa$ (MeV)	-0.284	-0.288	-0.315	-0.315
$\chi_\pi$	-0.45	-0.45	-0.55	-0.45
$\chi_\nu$	0.25	0.25	0.25	-0.45
$e^B$ (e b)	0.12	0.123	0.10	0.095
$g_\pi^B$ ( $\mu N$ )	1.0	1.0	1.3	1.3
$g_\nu^B$ ( $\mu N$ )	0.0	0.0	-0.2	0.3
Odd particle	$\pi$	$\pi$	$\nu$	$\nu$
$v_{j\rho}^2$	0.0303	0.03613	0.4317	0.0494
$\Gamma_0$ (MeV)	0.60	0.60	1.50	1.50
$\Lambda_0$ (MeV)	3.60	3.50	1.25	1.25
$A_0$ (MeV)	0.0	-0.5	-0.25	-0.05

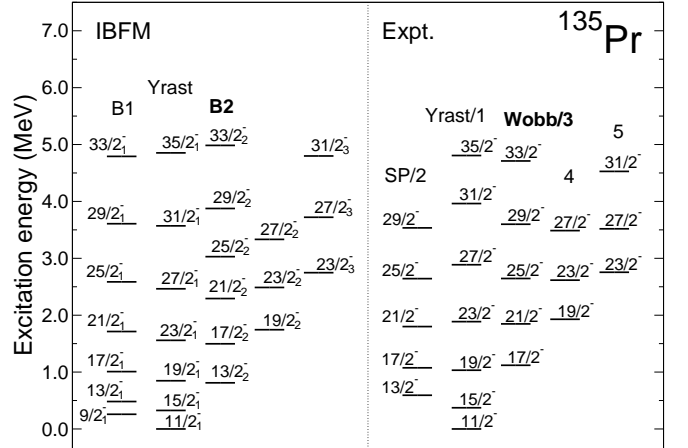


FIG. 3. Comparisons of theoretical and experimental lowest-lying negative-parity bands of  $^{135}\text{Pr}$ . The theoretical Yrast, first, and second excited bands are denoted by “Yrast”, “B1”, and “B2”, respectively. The experimental bands “SP” and “Wobb” denote the signature-partner and wobbling bands, respectively, that were identified in [8]. The notations “1” to “5” for the experimental bands corresponds to the ones used in Lv *et al.* [18]. The theoretical B2 band should be compared with the experimental Wobb band or band 3, both of which are highlighted in bold text.

B1, and B2 bands consist of the states that exhibit dominant  $\Delta I = 2$  inband  $E2$  transitions. The comparison between the experimental and theoretical energy spectra demonstrates that the IBFM describes well the observed [8, 18] low-lying bands in the odd-mass nucleus  $^{135}\text{Pr}$ .

For  $^{135}\text{Pr}$ , the experiment performed by Matta *et al.*



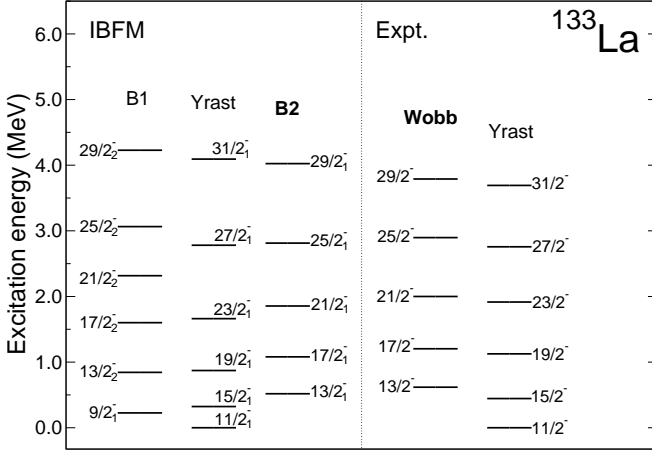


FIG. 4. Same as Fig. 3, but for  $^{133}\text{La}$ . The notations of the experimental bands are according to those used in Ref. [10].

[8] showed that beside the  $I = 11/2^-$  yrast band, the first excited band based on the  $13/2_1^-$  state can be identified as unfavored signature partner (SP) band, and the second excited band built on the  $17/2_2^-$  state can be assigned as an one-phonon wobbling band (denoted by “Wobb” in Fig. 3). In the IBFM, band B1 with bandhead  $9/2_1^-$  corresponds to the proposed SP band, and band B2 including the  $13/2_2^-$ ,  $17/2_2^-$  ... states is the theoretical counterpart of the proposed wobbling band.

As for  $^{135}\text{Pr}$ , two additional negative-parity bands have been considered in the new measurement by Lv *et al.* [18]: the first one comprising the  $19/2_2^-$ ,  $23/2_2^-$ , and  $27/2_2^-$  states (band 4 in Ref. [18] and Fig. 3), and the second one comprising the  $23/2_3^-$ ,  $27/2_3^-$ , and  $31/2_3^-$  states (band 5). The IBFM predicts additional two bands built on the  $19/2_2^-$  and  $23/2_3^-$  states, which are in agreement with the newly identified bands 4 and 5 in Ref. [18]. Our calculation shows that each of the two bands is composed by strong inband  $\Delta I = 2$   $E2$  transitions. In addition, the predicted interband  $B(E2; 23/2_3^- \rightarrow 19/2_2^-)$  transition is an order of magnitude weaker than the inband  $B(E2; 23/2_2^- \rightarrow 19/2_2^-)$  transition. This result supports the finding in the new measurement of Ref. [18], but is in contradiction to the earlier experiment of Ref. [9], in which the  $19/2_2^-$ ,  $23/2_3^-$ , and  $27/2_3^-$  states were grouped into a single band and interpreted as two-phonon wobbling band. The new bands proposed in Ref. [18] do not follow the  $I(I+1)$  energy dependence in a rotor picture, but appear to be rather vibrational, a fingerprint of the  $\gamma$  softness in this mass region.

Figures 4, 5, and 6 show the calculated and experimental three lowest-lying negative-parity bands of the odd-mass nuclei  $^{133}\text{La}$ ,  $^{127}\text{Xe}$ , and  $^{105}\text{Pd}$ . In general, the IBFM description of the observed low-lying band structure is satisfactory, except for the fact that the spins of the predicted bandhead states of some bands disagree

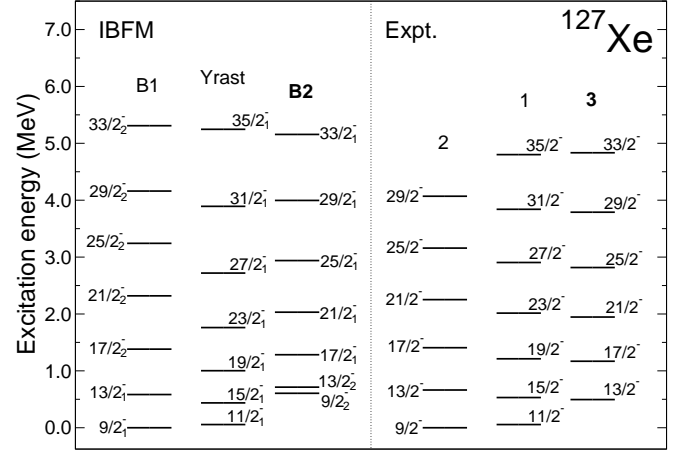


FIG. 5. Same as Fig. 3, but for  $^{127}\text{Xe}$ . The notations of the experimental bands are according to those used in Ref. [12].

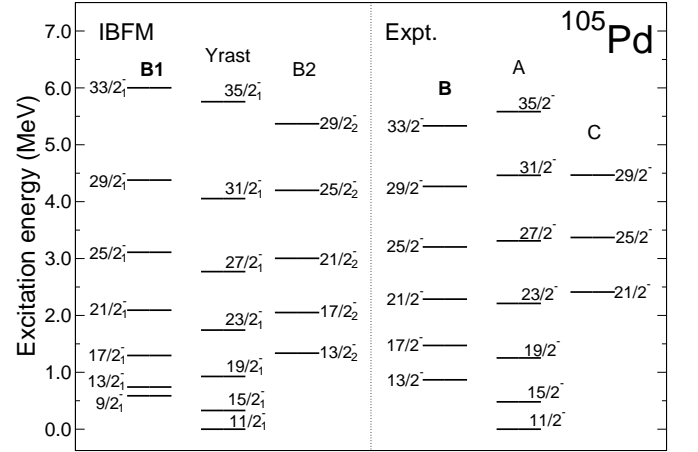


FIG. 6. Same as Fig. 3, but for  $^{105}\text{Pd}$ . The notations of the experimental bands are according to those used in Ref. [11].

with the experimental ones. The observed bandhead energies of the first (B1) and second (B2) excited bands are reproduced well by the IBFM.

For  $^{133}\text{La}$ , besides the  $11/2_1^-$  ground-state band, the experiment by Biswas *et al.* [10] identified the first excited band based on the  $13/2_1^-$  state as wobbling band. In Fig. 4, we associate the IBFM band B2 with bandhead  $13/2_1^-$  with the proposed wobbling band, according to the facts (i) that the calculated energy levels are in a better agreement with the experimental ones than band B1, (ii) that the spin of the bandhead state  $I = 13/2$  is correctly reproduced, and (iii) that, as shown later, the calculated  $B(E2)_{out}/B(E2)_{in}$  and  $B(M1)_{out}/B(E2)_{in}$  ratios are in a better agreement with data [10] than those for band B1.

The lowest three observed bands for  $^{127}\text{Xe}$  [12] are the lowest band (band 2) built on the  $9/2_1^-$  state, the first ex-

cited band (band 1) built on the  $I = 11/2^-$  state, and the second excited band (band 3) built on the  $13/2_1^-$  state, which was assigned to be wobbling band [12]. Band B2 in the IBFM consisting of the  $9/2_2^-$ ,  $13/2_2^-$ ,  $17/2_1^-$ ,  $21/2_1^-$ ,  $25/2_1^-$ , ... states is the theoretical counterpart of band 3. The IBFM yields band B1 with the bandhead  $9/2_1^-$  corresponding to the ground state, consistently with the observed band 2.

For  $^{105}\text{Pd}$ , Timár *et al.* [11] interpreted the first excited  $\Delta I = 2$  band (band B), which is built on the  $13/2_1^-$  state as wobbling band. This is the first evidence for a low-spin wobbling band in the mass  $A \approx 100$  region. The present IBFM calculation yields the equivalent  $\Delta I = 2$  band (B1) consisting of the  $9/2_1^-$ ,  $13/2_1^-$ , ... states.

### B. $E2/M1$ mixing ratio

The  $E2$  to  $M1$  mixing ratio  $\delta$  is a criterion for the wobbling interpretation, and is calculated by using the formula [51, 52]

$$\delta = 0.835 \times E_\gamma \frac{\langle I_f || \hat{T}^{(E2)} || I_i \rangle}{\langle I_f || \hat{T}^{(M1)} || I_i \rangle}, \quad (7)$$

where  $E_\gamma = E_{I_i} - E_{I_f}$ , with the resultant excitation energies of the initial  $I_i$  and final  $I_f$  states, and  $\langle I_f || \hat{T}^{(E2)} || I_i \rangle$  and  $\langle I_f || \hat{T}^{(M1)} || I_i \rangle$  represent reduced matrix elements of the  $E2$  and  $M1$  transition operators, respectively. The  $E2$  operator  $\hat{T}^{E2}$  here takes the form [21]:

$$\hat{T}^{(E2)} = \hat{T}_B^{(E2)} + \hat{T}_F^{(E2)}, \quad (8)$$

where

$$\hat{T}_B^{(E2)} = e_\pi^B \hat{Q}_\pi + e_\nu^B \hat{Q}_\nu, \quad (9)$$

and

$$\hat{T}_F^{(E2)} = -e^F \frac{1}{\sqrt{5}} (u_{j_\rho}^2 - v_{j_\rho}^2) Q_{j_\rho j_\rho} (a_{j_\rho}^\dagger \times \tilde{a}_{j_\rho})^{(2)} \quad (10)$$

are the bosonic and fermionic parts of the  $E2$  operators, respectively. Note that  $\hat{Q}_\rho$  has been defined in (2). We assume that the effective  $E2$  charges for proton  $e_\pi^B$  and neutron  $e_\nu^B$  bosons are equal to each other,  $e_\pi^B = e_\nu^B \equiv e^B$ , and fix  $e^B$  so that the experimental  $B(E2; 2_1^+ \rightarrow 0_1^+)$  rate of each even-even core nucleus is reproduced. For the fermion part, standard effective charge  $e^F = 1.5$  (0.5) eb is adopted for the odd proton (neutron). The  $M1$  transition operator  $\hat{T}^{(M1)}$  reads:

$$\hat{T}^{(M1)} = \hat{T}_B^{(M1)} + \hat{T}_F^{(M1)} \quad (11)$$

where

$$\hat{T}_B^{(M1)} = \sqrt{\frac{3}{4\pi}} (g_\pi^B \hat{L}_\pi + g_\nu^B \hat{L}_\nu), \quad (12)$$

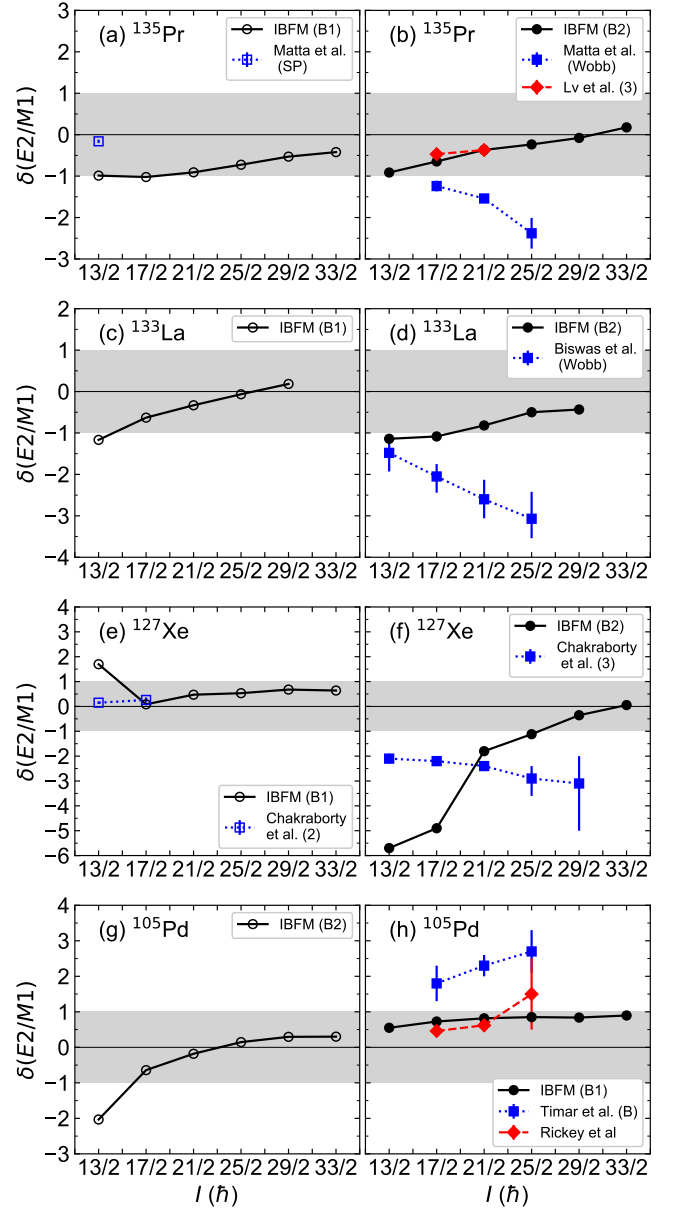


FIG. 7. The  $E2$  to  $M1$  mixing ratios  $\delta$  for the  $\Delta I = 1$  yrare to yrast transitions in the odd-mass nuclei  $^{135}\text{Pr}$ ,  $^{133}\text{La}$ ,  $^{127}\text{Xe}$ , and  $^{105}\text{Pd}$ , for which wobbling bands were previously suggested. The experimental values are taken from Refs. [8, 10–12, 18, 26]. The shaded area in each panel indicates  $|\delta| < 1$ . The notations of the experimental bands in each panel follow the ones used in the above references. The IBFM  $\delta$  values for those bands that were previously assigned to be wobbling bands are represented by solid symbols.

and

$$\hat{T}_F^{(M1)} = -\frac{1}{\sqrt{4\pi}} \langle j || g_l \mathbf{l} + g_s \mathbf{s} || j \rangle (a_{j_\rho}^\dagger \times \tilde{a}_{j_\rho})^{(1)} \quad (13)$$

are the boson and fermion parts of  $\hat{T}^{(M1)}$ , respectively. The effective gyromagnetic ( $g$ -)factors for the proton  $g_\pi^B$

and neutron  $g_\nu^B$  bosons are chosen to be close to the empirical values [53, 54] that satisfy  $g_\pi^B \approx 1.0 \mu_N$ , and  $g_\nu^B \approx 0 \mu_N$ . For the odd proton (neutron)  $g$ -factors, the standard Schmidt values  $g_l = 1.0 \mu_N$  and  $g_s = 5.58 \mu_N$  ( $g_l = 0 \mu_N$  and  $g_s = -3.82 \mu_N$ ) are used, with  $g_s$  quenched by 30% with respect to the free value. The adopted values of the boson effective  $E2$  charge  $e^B$ ,  $g$ -factors for proton  $g_\pi^B$  and neutron  $g_\nu^B$  are found in Table I.

We show in Fig. 7 the calculated  $\delta(E2/M1)$  ratios for the  $\Delta I = 1$  transitions between the yrast and yrare bands. The predicted  $\delta$  values for  $^{135}\text{Pr}$  shown in Figs. 7(a) and 7(b), are close to zero for both the B1  $\rightarrow$  Yrast and B2  $\rightarrow$  Yrast transitions. The experimental absolute values  $|\delta|$  for the Wobb  $\rightarrow$  Yrast transitions [8] increase with spin  $I$ . The updated data of Lv *et al.* [18], however, provide smaller mixing ratios for the same band (band 3) at  $I = 17/2$  and  $21/2$ , which agree with the present calculations.

The computed mixing ratios for  $^{133}\text{La}$ , shown in Figs. 7(c) and 7(d), are generally small,  $|\delta| < 1$ . The measured  $\delta$  ratios for the wobbling (Wobb) band, which are the basis of the wobbling interpretation of the  $13/2^-$  band, are depicted in Fig. 7(d). The corresponding IBFM  $\delta$  values for the B2  $\rightarrow$  Yrast transitions, plotted also in Fig. 7(d), are much smaller in magnitude than these experimental values, but are rather close to those obtained with the quasiparticle-plus-triaxial-rotor (QTR) model [10], giving more weight to a non-wobbling description of the band. We note that the interpretation of the experimental  $13/2^-$  band as wobbling band [10] has been recently questioned in Ref. [55], with respect to the reported  $E2$  dominance of the transitions connecting the proposed wobbling and normal bands.

The calculated  $\delta$  for the B1  $\rightarrow$  Yrast transitions for  $^{127}\text{Xe}$  shown in Fig. 7(e) are small, except for the one at  $I = 13/2$ . As seen in Fig. 7(f), the absolute  $\delta$  ratios for the B2  $\rightarrow$  Yrast transitions are predicted to be smaller in magnitude than the experimental counterparts for  $I \geq 21/2$ . However, the predicted ratios are unusually large  $|\delta| \approx 5$  for  $I < 21/2$ . An earlier in-beam spectroscopic study by Urban *et al.* [56] gave the mixing ratio  $\delta = -1.7^{+0.4}_{-0.6}$  or  $-0.45 \pm 0.12$  for the  $E_\gamma = 483$  keV (or  $13/2^-_1 \rightarrow 11/2^-_1$ ) decay for  $^{127}\text{Xe}$ , the absolute value of which is considerably overestimated by the present calculation. As we show later, the too large  $|\delta|$  is here obtained because the calculated  $M1$  matrix elements for  $^{127}\text{Xe}$ , especially the one for the  $13/2^-_2 \rightarrow 11/2^-_1$  transition, are negligibly small. For  $^{127}\text{Xe}$ , the  $1h_{11/2}$  single-neutron orbital is nearly half filled,  $v_{j_\nu}^2 \approx 0.5$  (see Table I), in which case the contributions from both the dynamical and exchange terms of  $\hat{V}_{\text{BF}}$  are rather sensitive to the choice of their strength parameters. The chosen set of the strength parameters might have yield substantial amount of configuration mixing in the lower spin states, thus resulting in the too small  $M1$  matrix elements.

The absolute values of the calculated  $\delta$  for both bands B1 and B2 for  $^{105}\text{Pd}$  shown in Figs. 7(g) and 7(h), are

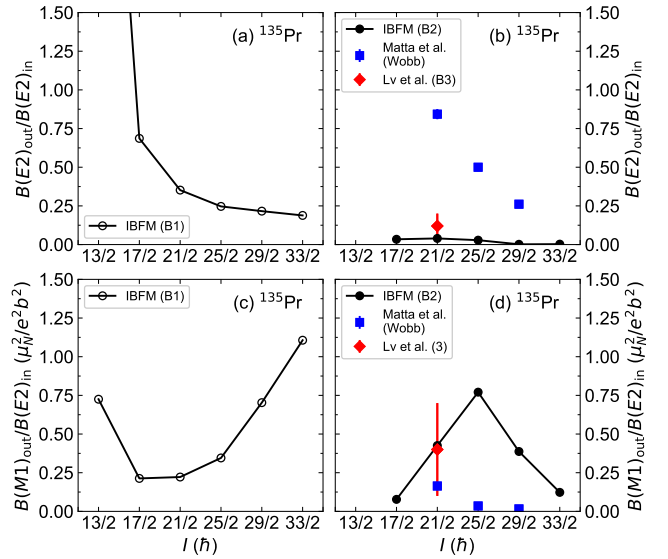


FIG. 8. The calculated ratios  $B(E2; I \rightarrow I-1)_{\text{out}}/B(E2; I \rightarrow I-2)_{\text{in}}$ , and  $B(M1; I \rightarrow I-1)_{\text{out}}/B(E2; I \rightarrow I-2)_{\text{in}}$  as functions of spin  $I$  for the B1  $\rightarrow$  Yrast and B2  $\rightarrow$  Yrast transitions of  $^{135}\text{Pr}$ . The notations of the experimental bands correspond to those used in Refs. [8, 18]. The experimental band built on the  $17/2^-_2$  state was identified as wobbling band in [8], and is denoted here by “Wobb”.

all less than one except for the lowest  $I = 13/2$  state of band B2. The calculated  $\delta$  values for band B1 are by a factor of two to three smaller than the measured values for the proposed wobbling band B [11]. In contrast, the mixing ratios obtained by Rickey *et al.* [26], also shown in Fig. 7(h), agree with the calculated values at  $I = 17/2$  and  $21/2$ . In this case we are again faced with contradicting experimental values, like in the case of  $^{135}\text{Pr}$ , which keeps open the question of the real nature of the band.

### C. $B(E2)$ and $B(M1)$ transitions

In Fig. 8 we show the predicted  $B(E2)_{\text{out}}/B(E2)_{\text{in}}$  ( $B(M1)_{\text{out}}/B(E2)_{\text{in}}$ ) ratios of the interband  $\Delta I = 1$   $E2$  ( $M1$ ) to the inband  $\Delta I = 2$   $E2$  transitions for the bands B1 and B2 for  $^{135}\text{Pr}$ . We see from Fig. 8(b) that, as compared to the B1  $\rightarrow$  Yrast  $E2$  transitions, the predicted B2  $\rightarrow$  Yrast  $E2$  transitions are generally weak. The calculated  $B(E2)_{\text{out}}/B(E2)_{\text{in}}$  ratios for band B2 are much smaller than the experimental data reported by Matta *et al.* [8], but are closer to the new data of Lv *et al.* [18] at  $I = 21/2$ . The calculated  $B(M1)_{\text{out}}/B(E2)_{\text{in}}$  ratios for band B2, shown in Fig. 8(d), are much larger than the data reported in [8], but are in a better agreement with the new value at  $I = 21/2$  [18].

The ratios  $B(E2)_{\text{out}}/B(E2)_{\text{in}}$  and  $B(M1)_{\text{out}}/B(E2)_{\text{in}}$  for  $^{133}\text{La}$  are shown in Fig. 9. The predicted  $B(E2)_{\text{out}}/B(E2)_{\text{in}}$  ratios for the B2  $\rightarrow$  Yrast transitions

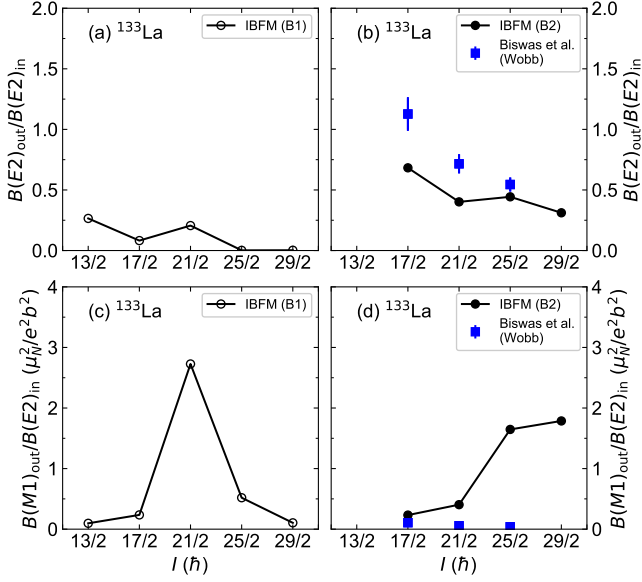


FIG. 9. Same as Fig. 8, but for  $^{133}\text{La}$ . The experimental data are from [10], which identified the yrare band as wobbling band (denoted by “Wobb”).

agree with the experimental values reported in Ref. [10] (Fig. 9(b)), in which the first excited band (denoted as “Wobb” in Figs. 4 and 9) has been interpreted as wobbling band, as well as with the QTR model calculations [10]. The  $B(M1)_{\text{out}}/B(E2)_{\text{in}}$  ratios for the B2  $\rightarrow$  Yrast transition are calculated to be much larger than the measured values of the Wobb  $\rightarrow$  Yrast transitions (Fig. 9(d)), but rather agree with the QTR results [10], which also overestimated the data.

As for  $^{127}\text{Xe}$ , the calculated  $B(E2)_{\text{out}}/B(E2)_{\text{in}}$ , shown in Fig. 10(b), are much smaller than the experimental ones for band 3, which was assigned to be wobbling band [12]. The experimental  $B(E2)_{\text{out}}/B(E2)_{\text{in}}$  ratios indicate strong  $E2$  transitions from band 3 to the yrast band (band 1 in Fig. 5), especially for the spin  $I \geq 21/2$ , while the errors are also large. In Fig. 10(d), the predicted  $B(M1)_{\text{out}}/B(E2)_{\text{in}}$  ratios for the band B2 at  $I = 17/2$  and  $21/2$  are considerably smaller than the experimental values for band 3, which was identified as wobbling band. We recall that the too large  $\delta$  values are calculated at these spins (see Fig. 7(f)).

The  $B(E2)_{\text{out}}/B(E2)_{\text{in}}$  ratios for both the B1  $\rightarrow$  Yrast and B2  $\rightarrow$  Yrast transitions in  $^{105}\text{Pd}$  shown in Fig. 11 are relatively small, in comparison to the measured values for band B [11], which was interpreted as the wobbling band. Generally, the  $B(M1)_{\text{out}}/B(E2)_{\text{in}}$  ratios are calculated to be larger than the data. Thus we can confirm the M1 dominance of the predicted transitions between yrare and yrast bands for  $^{105}\text{Pd}$ .

For the sake of completeness, the calculated values for the mixing ratios  $\delta$ , the  $B(M1)_{\text{out}}/B(E2)_{\text{in}}$ , the  $B(E2)_{\text{out}}/B(E2)_{\text{in}}$  ratios of the lowest two excited

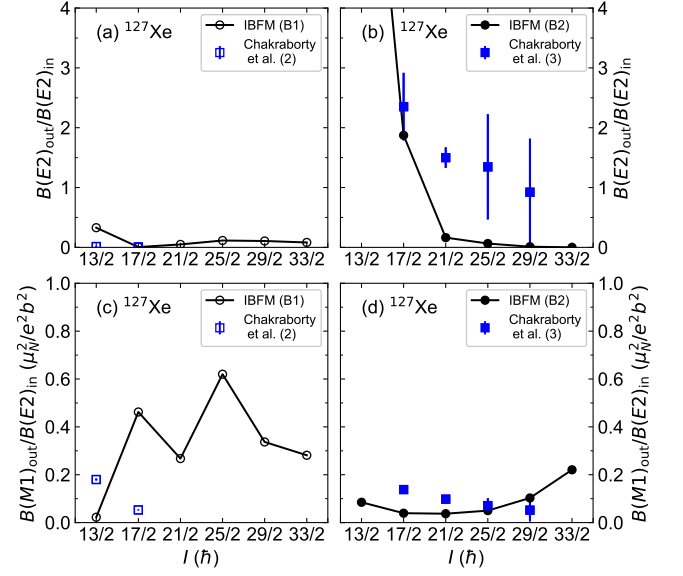


FIG. 10. Same as Fig. 9, but for  $^{127}\text{Xe}$ . The experimental data are from [12], which identified the  $I = 13/2^-$  band (3) as wobbling band.

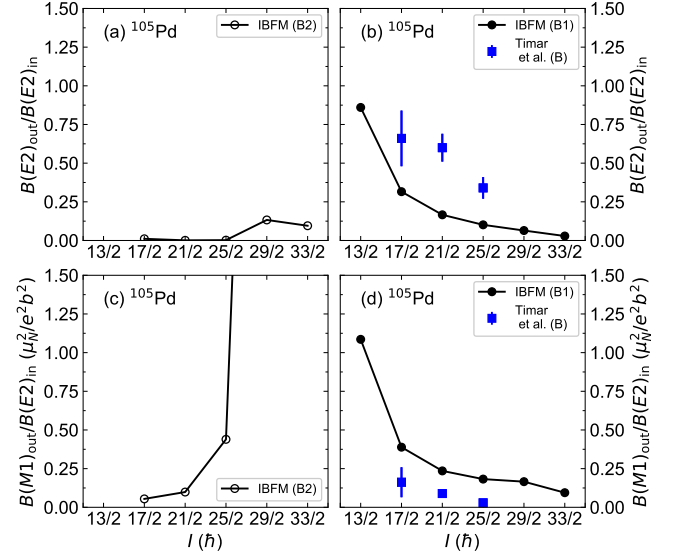


FIG. 11. Same as Fig. 9, but for  $^{105}\text{Pd}$ . The experimental band (B), built on the  $13/2^-$  state, was identified as wobbling band in [11].

bands, and the corresponding experimental values based on the wobbling interpretation of the yrare bands [8, 10–12], and those from the new measurement for  $^{135}\text{Pr}$  [18] and the old experimental  $\delta$  values for  $^{105}\text{Pd}$  [26] are listed in Table II.



TABLE II. Comparisons between the calculated and experimental  $\delta(E2/M1)$  mixing ratios of the  $\Delta I = 1$  interband transitions, and the ratios of the interband  $B(M1; I \rightarrow I - 1)_{out}$  and  $B(E2; I \rightarrow I - 1)_{out}$  to inband  $B(E2; I \rightarrow I - 2)_{in}$  transition rates, connecting the low-lying yrare bands to the yrast bands in  $^{135}\text{Pr}$ ,  $^{133}\text{La}$ ,  $^{127}\text{Xe}$ , and  $^{105}\text{Pd}$ .

Nucleus	$E_\gamma$ (keV)	Spin	$\delta$		$B(M1)_{out}/B(E2)_{in}$		$B(E2)_{out}/B(E2)_{in}$	
			EXP	IBFM	EXP	IBFM	EXP	IBFM
$^{135}\text{Pr}$ [8]	747.0	$17/2_1^-$	$-1.24 \pm 0.13$	-0.646		0.078		0.034
	812.8	$21/2_1^-$	$-1.54 \pm 0.09$	-0.368	$0.164 \pm 0.014$	0.425	$0.843 \pm 0.032$	0.040
	754.6	$25/2_1^-$	$-2.38 \pm 0.37$	-0.236	$0.035 \pm 0.009$	0.771	$0.500 \pm 0.025$	0.028
	710.2	$29/2_1^-$		-0.078	$\leq 0.016 \pm 0.004$	0.387	$\geq 0.261 \pm 0.014$	0.0017
	593.9	$13/2_1^-$	$-0.16 \pm 0.04$	-0.988		0.725		4.371
$^{135}\text{Pr}$ [18]	747.3	$17/2_1^-$	$-0.47^{+0.09}_{-0.22}$	-0.646		0.078		0.034
	813.2	$21/2_1^-$	$-0.37^{+0.10}_{-0.14}$	-0.368	$0.4 \pm 0.3$	0.425	$0.12 \pm 0.08$	0.040
$^{133}\text{La}$ [10]	618	$13/2_1^-$	$-1.48^{+0.45}_{-0.32}$	-1.167				
	758	$17/2_1^-$	$-2.05^{+0.39}_{-0.30}$	-0.630	$0.107^{+0.035}_{-0.028}$	0.232	$1.127^{+0.140}_{-0.130}$	0.683
	874	$21/2_1^-$	$-2.60^{+0.46}_{-0.47}$	-0.331	$0.056^{+0.018}_{-0.019}$	0.404	$0.716^{+0.079}_{-0.079}$	0.401
	982	$25/2_1^-$	$-3.07^{+0.47}_{-0.65}$	-0.065	$0.039^{+0.011}_{-0.015}$	1.646	$0.545^{+0.057}_{-0.059}$	0.443
$^{127}\text{Xe}$ [12]	483	$13/2_1^-$	$-2.1^{+0.2}_{-0.2}$	-5.699		0.085		9.242
	639	$17/2_1^-$	$-2.2^{+0.2}_{-0.1}$	-4.901	$0.138 \pm 0.012$	0.039	$2.352 \pm 0.565$	1.874
	735	$21/2_1^-$	$-2.4^{+0.1}_{-0.1}$	-1.801	$0.098 \pm 0.005$	0.037	$1.500 \pm 0.172$	0.163
	800	$25/2_1^-$	$-2.9^{+0.7}_{-0.3}$	-1.117	$0.071 \pm 0.031$	0.050	$1.346 \pm 0.879$	0.064
	884	$29/2_1^-$	$-3.1^{+1.3}_{-1.1}$	-0.355	$0.052 \pm 0.044$	0.103	$0.922 \pm 0.895$	0.011
	651	$13/2_2^-$	$+0.15^{+0.05}_{-0.05}$	+1.698	$0.180 \pm 0.004$	0.022	$0.014 \pm 0.009$	0.329
	876	$17/2_2^-$	$+0.26^{+0.10}_{-0.10}$	+0.085	$0.053 \pm 0.002$	0.462	$0.007 \pm 0.005$	0.005
$^{105}\text{Pd}$ [11]	991	$17/2_1^-$	$+1.8 \pm 0.5$	+0.727	$0.162 \pm 0.097$	0.316	$0.66 \pm 0.18$	0.389
	1034	$21/2_1^-$	$+2.3 \pm 0.3$	+0.817	$0.089 \pm 0.026$	0.166	$0.60 \pm 0.09$	0.236
	994	$25/2_1^-$	$+2.7 \pm 0.6$	+0.851	$0.029 \pm 0.057$	0.101	$0.34 \pm 0.07$	0.182
$^{105}\text{Pd}$ [26]	991	$17/2_1^-$	$+0.46 \pm 0.10$	+0.727		0.316		0.389
	1034	$21/2_1^-$	$+0.62 \pm 0.18$	+0.817		0.166		0.236
	994	$25/2_1^-$	$+1.5 \pm 1.0$	+0.851		0.101		0.182

#### D. Boson and fermion contributions to matrix elements

In this section, we study the individual contributions of the boson and fermion parts of the  $E2$  (8) and  $M1$  (11) transition operators to the relevant matrix elements. In Figs. 12 and 13, we show the corresponding reduced matrix elements of the bosonic and fermionic  $E2$  ( $M1$ ) operators,  $\langle I - 1 || \hat{T}_B^{(E2)} || I \rangle$  and  $\langle I - 1 || \hat{T}_F^{(E2)} || I \rangle$  ( $\langle I - 1 || \hat{T}_B^{(M1)} || I \rangle$  and  $\langle I - 1 || \hat{T}_F^{(M1)} || I \rangle$ ), and the absolute values of the full matrix elements  $|\langle I - 1 || \hat{T}^{(E2)} || I \rangle|$  ( $|\langle I - 1 || \hat{T}^{(M1)} || I \rangle|$ ), for the  $\Delta I = 1$  interband transitions from the theoretical bands B1 and B2 to yrast bands, respectively. We observe in these figures that, in general, boson contributions are dominant in the  $E2$  matrix elements, for both bands B1 and B2, and for all the nuclei considered. In all cases, the boson and fermion parts contribute coherently to the  $E2$  matrix elements. On the other hand, the fermion part plays an important role mainly in the  $M1$  matrix elements, especially, those for band B1 of  $^{135}\text{Pr}$  and band B2 of  $^{133}\text{La}$  (see Figs. 12(e) and 13(f)).

For band B1 of  $^{135}\text{Pr}$  the fermion contribution to the  $M1$  matrix elements is systematically larger than, and is opposite in sign to the boson one. As for band B2 of  $^{135}\text{Pr}$ , which is here associated with the proposed wobbling band [8], both the boson and fermion parts make

small in magnitude, but coherent contributions to the  $E2$  and  $M1$  matrix elements. Band B1 (B2) of  $^{133}\text{La}$  appears to show similar patterns of the boson and fermion contributions to the matrix elements to those of band B2 (B1) of  $^{135}\text{Pr}$ . We note that band B2 of  $^{133}\text{La}$  is here considered to be the theoretical counterpart of the proposed wobbling band [10] (see Fig. 4), while both bands B1 and B2 in the same nucleus are shown to be close in energy (see Fig. 4) and have similar electromagnetic properties (see Figs. 7(c,d) and 9). There is essentially no fermion contribution to the  $E2$ , as well as  $M1$ , matrix elements of both bands B1 and B2 of  $^{127}\text{Xe}$ . For this nucleus, the calculated  $M1$  matrix elements at  $I = 13/2$  are especially small, and this corroborates the too large  $\delta$  mixing ratios at lower spins (see Figs. 7(e) and 7(f)). For band B1 of  $^{105}\text{Pd}$ , here associated with the wobbling band [11], the boson and fermion parts make coherent contributions to the matrix elements (see Figs. 12(d) and 12(h)). This systematic trend is similar to the one observed for band B2 of  $^{135}\text{Pr}$ , which is also associated with the wobbling band in the present study. The boson contribution to band B2 of  $^{105}\text{Pd}$  becomes increasingly larger for higher spin.

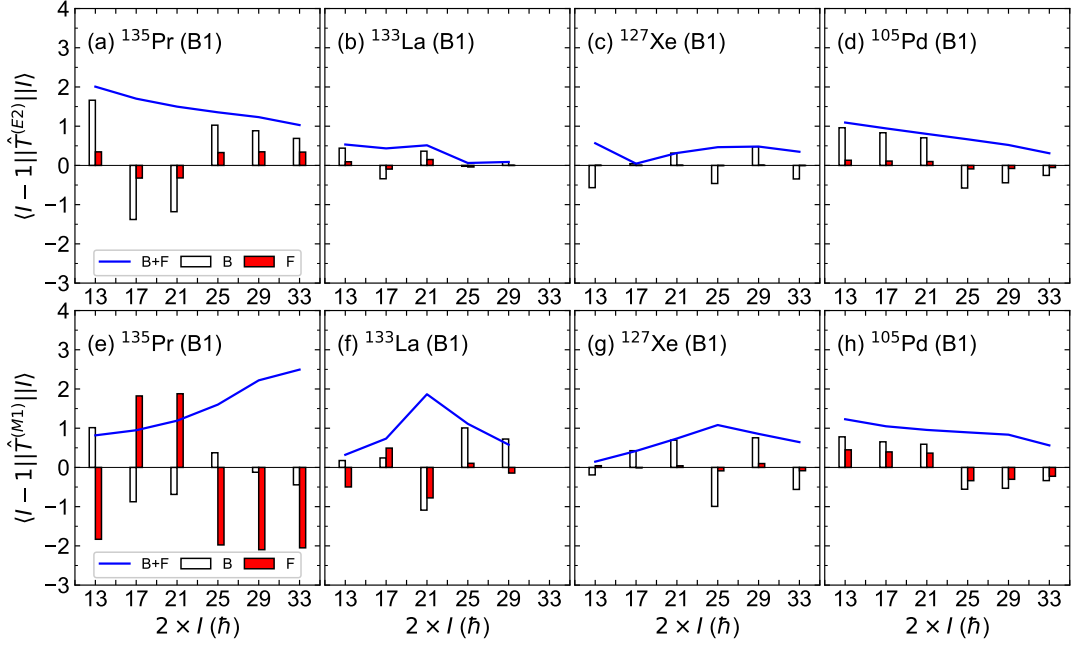


FIG. 12. The bosonic and fermionic reduced matrix elements of the  $E2$ ,  $\hat{T}^{(E2)}$  (8), (upper row) and  $M1$ ,  $\hat{T}^{(M1)}$  (11), (lower row) operators for the  $\Delta I = 1$  interband transition from bands B1 to yrast bands of  $^{135}\text{Pr}$ ,  $^{133}\text{La}$ ,  $^{127}\text{Xe}$ , and  $^{105}\text{Pd}$ , plotted for each angular momentum  $I$ . The absolute values of the reduced matrix elements of  $\hat{T}^{(E2)}$  and  $\hat{T}^{(M1)}$  are also shown. The theoretical band B1 for  $^{105}\text{Pd}$  is here associated with the proposed wobbling band in Ref. [11].

### E. The gold nuclei

Finally, we make a remark on the recently proposed wobbling bands in the heavier nuclei, i.e.,  $^{187}\text{Au}$  [13] and  $^{183}\text{Au}$  [14]. Empirically, their low-lying negative-parity states are understood as the proton  $\pi h_{9/2}$  orbital coupled with a prolate-deformed core. Within the standard IBFM, the above nuclei would be described by the coupling between the odd proton  $\pi h_{11/2}$  orbital and the even-even Hg core. Earlier phenomenological IBFM calculations [57, 58] considered the  $\pi h_{9/2}$  intruder orbital coupled to the even-even Pt core in order to describe the  $I = 9/2^-$  ground state bands of odd-mass Au nuclei. In principle, both the  $\pi h_{11/2}$  and  $\pi h_{9/2}$  orbitals could be simultaneously included in our model but, due to the huge energy difference between their spherical single-particle levels across the proton  $Z = 82$  major shell gap, contribution from the latter is expected to be negligible. In addition, the even-even core nuclei  $^{188}\text{Hg}$  and  $^{184}\text{Hg}$  are often characterized by oblate and prolate shapes that coexist near the ground state [59]. Previous mean-field calculations using the Skyrme [60] and Gogny [61] forces predicted an oblate minimum for  $^{188}\text{Hg}$  and a pronounced prolate-oblate shape coexistence for  $^{184}\text{Hg}$ . In both cases, the PESs were shown to be far from  $\gamma$  soft, in contrast to the nuclei considered here (see Fig. 1). These facts indicate a potential difficulty in the treatment of the  $\pi h_{11/2}$  orbital for  $^{187}\text{Au}$  and  $^{183}\text{Au}$  within our model calculations.

tions.

## IV. CONCLUDING REMARKS

In summary, an alternative interpretation of the recently reported low-spin wobbling bands in the odd-mass nuclei  $^{135}\text{Pr}$ ,  $^{133}\text{La}$ ,  $^{127}\text{Xe}$ , and  $^{105}\text{Pd}$  has been presented through IBFM calculations. The bosonic Hamiltonian for the even-even core nuclei, and the essential building blocks of the boson-fermion interaction have been determined by using the constrained mean-field approach based on a given nuclear EDF. The PESs for the even-even core nuclei, obtained from the mean-field calculations with representative classes of the universal EDF, generally exhibit pronounced  $\gamma$  softness characteristic for nonaxial nuclei. The calculated  $E2$  to  $M1$  mixing ratios  $\delta$  for the  $\Delta I = 1$  transitions between the yrare and yrast bands in the considered nuclei are consistently small,  $|\delta| < 1$ . These mixing ratios indicate the  $M1$  dominance of the transitions connecting the yrare bands in question to the yrast bands, which is in contradiction with the wobbling interpretation, and are in agreement with the updated experimental mixing ratios for  $^{135}\text{Pr}$  [18] and the old data for  $^{105}\text{Pd}$  [26]. This work sheds new light upon the excited low-lying bands in  $\gamma$ -soft nuclei, questioning their wobbling interpretation.

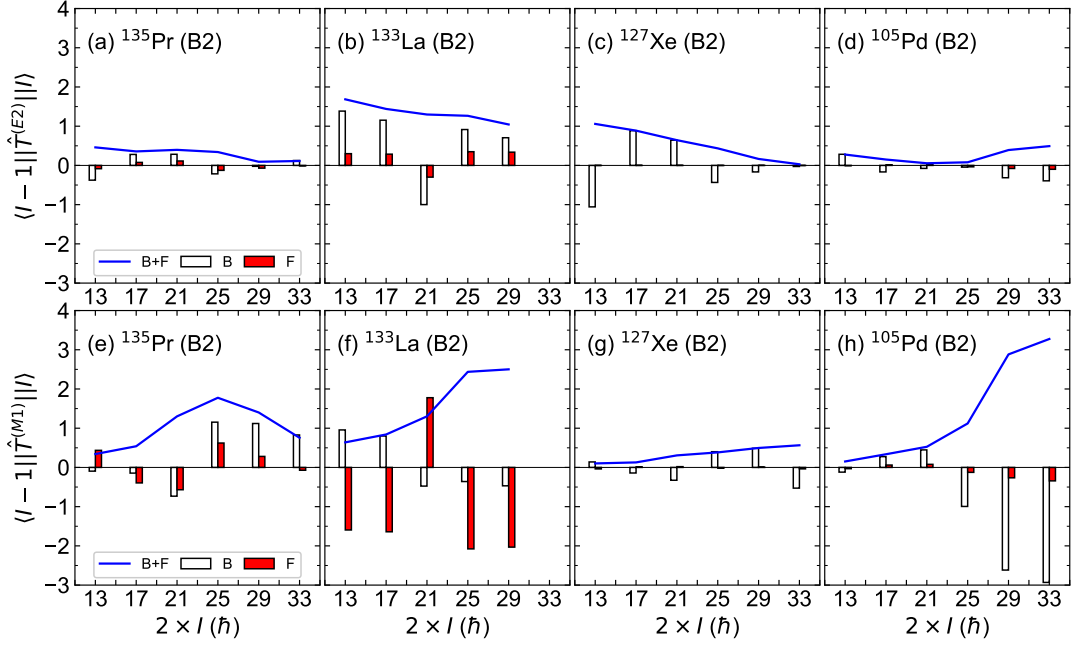


FIG. 13. The same as Fig. 12, but for the transitions from bands B2 to yrast bands. The theoretical bands B2 for  $^{135}\text{Pr}$ ,  $^{133}\text{La}$ , and  $^{127}\text{Xe}$  are here associated with the proposed wobbling bands in Refs. [8, 10, 12], respectively.

## ACKNOWLEDGMENTS

The authors thank E. A. Lawrie for valuable comments. The work of K.N. is supported by the Tenure

Track Pilot Programme of the Croatian Science Foundation and the École Polytechnique Fédérale de Lausanne, and the Project TTP-2018-07-3554 Exotic Nuclear Structure and Dynamics, with funds of the Croatian-Swiss Research Programme.

- 
- [1] A. Bohr and B. R. Mottelson, *Nuclear Structure*, Vol. II (Benjamin, New York, USA, 1975).
  - [2] S. W. Odegård *et al.*, *Phys. Rev. Lett.* **86**, 5866 (2001).
  - [3] D. R. Jensen *et al.*, *Phys. Rev. Lett.* **89**, 142503 (2002).
  - [4] G. Schönwaßer *et al.*, *Phys. Lett. B* **552**, 9 (2003).
  - [5] H. Amro *et al.*, *Phys. Lett. B* **553**, 197 (2003).
  - [6] P. Bringel *et al.*, *Eur. Phys. J. A* **24**, 167 (2005).
  - [7] D. J. Hartley *et al.*, *Phys. Rev. C* **80**, 041304 (2009).
  - [8] J. T. Matta *et al.*, *Phys. Rev. Lett.* **114**, 082501 (2015).
  - [9] N. Sensharma *et al.*, *Phys. Lett. B* **792**, 170 (2019).
  - [10] S. Biswas *et al.*, *Eur. Phys. J. A* **55**, 159 (2019).
  - [11] J. Timár *et al.*, *Phys. Rev. Lett.* **122**, 062501 (2019).
  - [12] S. Chakraborty *et al.*, *Phys. Lett. B* **811**, 135854 (2020).
  - [13] N. Sensharma *et al.*, *Phys. Rev. Lett.* **124**, 052501 (2020).
  - [14] S. Nandi *et al.*, *Phys. Rev. Lett.* **125**, 132501 (2020).
  - [15] Q. B. Chen, S. Frauendorf, and C. M. Petrache, *Phys. Rev. C* **100**, 061301(R) (2019).
  - [16] F.-Q. Chen and C. M. Petrache, *Phys. Rev. C* **103**, 064319 (2021).
  - [17] S. Guo *et al.*, to be published, <https://arxiv.org/abs/2011.143549>.
  - [18] B. F. Lv *et al.*, *Phys. Lett. B* **824**, 136840 (2022).
  - [19] S. Frauendorf and F. Döna, *Phys. Rev. C* **89**, 014322 (2014).
  - [20] F. Iachello and O. Scholten, *Phys. Rev. Lett.* **43**, 679 (1979).
  - [21] F. Iachello and P. Van Isacker, *The interacting boson-fermion model* (Cambridge University Press, Cambridge, 1991).
  - [22] M. Bender, P.-H. Heenen, and P.-G. Reinhard, *Rev. Mod. Phys.* **75**, 121 (2003).
  - [23] D. Vretenar, A. Afanasjev, G. Lalazissis, and P. Ring, *Phys. Rep.* **409**, 101 (2005).
  - [24] L. M. Robledo, T. R. Rodríguez, and R. R. Rodríguez-Guzmán, *J. Phys. G: Nucl. Part. Phys.* **46**, 013001 (2019).
  - [25] N. Schunck, ed., *Energy Density Functional Methods for Atomic Nuclei*, 2053-2563 (IOP Publishing, 2019).
  - [26] F. A. Rieck, J. A. Grau, L. E. Samuelson, and P. C. Simms, *Phys. Rev. C* **15**, 1530 (1977).
  - [27] A. Leviatan, *Phys. Lett. B* **209**, 415 (1988).
  - [28] C. Alonso, J. Arias, F. Iachello, and A. Vitturi, *Nucl. Phys. A* **539**, 59 (1992).
  - [29] F. Iachello, A. Leviatan, and D. Petrellis, *Phys. Lett. B* **705**, 379 (2011).
  - [30] M. Büyükat, C. E. Alonso, J. M. Arias, L. Fortunato, and A. Vitturi, *Symmetry* **13**, 10.3390/sym13020215 (2021).

- [31] S. Goriely, S. Hilaire, M. Girod, and S. Péru, *Phys. Rev. Lett.* **102**, 242501 (2009).
- [32] T. Nikšić, D. Vretenar, and P. Ring, *Phys. Rev. C* **78**, 034318 (2008).
- [33] K. Nomura, R. Rodríguez-Guzmán, and L. M. Robledo, *Phys. Rev. C* **96**, 064316 (2017).
- [34] A. Bohr, *Mat. Fys. Medd. Dan. Vid. Selsk.* **27**, 16 (1953).
- [35] F. Iachello and A. Arima, *The interacting boson model* (Cambridge University Press, Cambridge, 1987).
- [36] P. Ring and P. Schuck, *The nuclear many-body problem* (Berlin: Springer-Verlag, 1980).
- [37] A. Bohr and B. R. Mottelson, *Nuclear structure* (1975).
- [38] J. Decharge and M. Girod and D. Gogny, *Phys. Lett. B* **55**, 361 (1975).
- [39] Y. Tian, Z. Y. Ma, and P. Ring, *Phys. Lett. B* **676**, 44 (2009).
- [40] L. Wilets and M. Jean, *Phys. Rev.* **102**, 788 (1956).
- [41] T. Otsuka, A. Arima, and F. Iachello, *Nucl. Phys. A* **309**, 1 (1978).
- [42] J. N. Ginocchio and M. W. Kirson, *Nucl. Phys. A* **350**, 31 (1980).
- [43] M. A. Caprio and F. Iachello, *Phys. Rev. Lett.* **93**, 242502 (2004).
- [44] M. Caprio and F. Iachello, *Annals of Physics* **318**, 454 (2005).
- [45] K. Nomura, N. Shimizu, and T. Otsuka, *Phys. Rev. Lett.* **101**, 142501 (2008).
- [46] K. Nomura, N. Shimizu, D. Vretenar, T. Nikšić, and T. Otsuka, *Phys. Rev. Lett.* **108**, 132501 (2012).
- [47] O. Scholten, *Prog. Part. Nucl. Phys.* **14**, 189 (1985).
- [48] F. Iachello, ed., *Interacting Bose-Fermi Systems in Nuclei* (Springer, New York, 1981).
- [49] K. Nomura, T. Nikšić, and D. Vretenar, *Phys. Rev. C* **93**, 054305 (2016).
- [50] T. Otsuka and N. Yoshida, (1985), JAERI-M (Japan Atomic Energy Research Institute) Report No. 85.
- [51] K. S. Krane and R. M. Steffen, *Phys. Rev. C* **2**, 724 (1970).
- [52] J. Lange, K. Kumar, and J. H. Hamilton, *Rev. Mod. Phys.* **54**, 119 (1982).
- [53] M. Sambataro, O. Scholten, A. Dieperink, and G. Piccitto, *Nucl. Phys. A* **423**, 333 (1984).
- [54] N. Yoshida and F. Iachello, *Prog. Theor. Exp. Phys.* **2013**, 043D01 (2013).
- [55] W. Hua, S. Guo, and C. Petrache, to be published, <https://arxiv.org/abs/2011.14369>.
- [56] W. Urban, T. Morek, C. Droste, B. Kotliński, J. Srebrny, J. Wrzesiński, and J. Styczeń, *Z. Phys. A* **320**, 327 (1984).
- [57] R. Bijker and A. Dieperink, *Nucl. Phys. A* **379**, 221 (1982).
- [58] J. M. Arias, C. E. Alonso, and M. Lozano, *Phys. Rev. C* **33**, 1482 (1986).
- [59] K. Heyde and J. L. Wood, *Rev. Mod. Phys.* **83**, 1467 (2011).
- [60] J. M. Yao, M. Bender, and P.-H. Heenen, *Phys. Rev. C* **87**, 034322 (2013).
- [61] K. Nomura, R. Rodríguez-Guzmán, and L. M. Robledo, *Phys. Rev. C* **87**, 064313 (2013).